Cell

UAP56 Couples piRNA Clusters to the Perinuclear Transposon Silencing Machinery

Fan Zhang,[1,2,8] Jie Wang,[3,8] Jia Xu,[3] Zhao Zhang,[1,2] Birgit S. Koppetsch,[1,2] Nadine Schultz,[1,2] Thom Vreven,[3] Carine Meignin,[4] Ilan Davis,[5] Phillip D. Zamore,[6,7] Zhiping Weng,[3,*] and William E. Theurkauf[1,2,*]
[1]Program in Cell and Developmental Dynamics
[2]Program in Molecular Medicine
[3]Program in Bioinformatics and Integrative Biology
University of Massachusetts Medical School, Worcester, MA 01655, USA
[4]Centre National de la Recherche Scientifique, Unité Propre de Recherche 9022, Institut de Biologie Moléculaire et Cellulaire, Université de Strasbourg, 67 084 Strasbourg Cedex, France
[5]Department of Biochemistry, The University of Oxford, South Parks Road, Oxford OX1 3QU, UK
[6]Department of Biochemistry and Molecular Pharmacology, University of Massachusetts Medical School, Worcester, MA 01655, USA
[7]Howard Hughes Medical Institute
[8]These authors contributed equally to this work
*Correspondence: zhiping.weng@umassmed.edu (Z.W.), william.theurkauf@umassmed.edu (W.E.T.)
http://dx.doi.org/10.1016/j.cell.2012.09.040

SUMMARY

piRNAs silence transposons during germline development. In *Drosophila*, transcripts from heterochromatic clusters are processed into primary piRNAs in the perinuclear nuage. The nuclear DEAD box protein UAP56 has been previously implicated in mRNA splicing and export, whereas the DEAD box protein Vasa has an established role in piRNA production and localizes to nuage with the piRNA binding PIWI proteins Ago3 and Aub. We show that UAP56 colocalizes with the cluster-associated HP1 variant Rhino, that nuage granules containing Vasa localize directly across the nuclear envelope from cluster foci containing UAP56 and Rhino, and that cluster transcripts immunoprecipitate with both Vasa and UAP56. Significantly, a charge-substitution mutation that alters a conserved surface residue in UAP56 disrupts colocalization with Rhino, germline piRNA production, transposon silencing, and perinuclear localization of Vasa. We therefore propose that UAP56 and Vasa function in a piRNA-processing compartment that spans the nuclear envelope.

INTRODUCTION

Transposons are ubiquitous genome pathogens that can mobilize and induce mutations that alter gene expression, cause disease, and drive evolution (Bennetzen, 2000; Britten, 2010; Hedges and Belancio, 2011). The 23–30 nucleotide (nt) long piRNAs, which guide sequence-specific RNA cleavage by PIWI clade Argonaute proteins in vitro, silence transposons during germline development (Aravin et al., 2007; Ghildiyal and Zamore, 2009; Gunawardane et al., 2007; Khurana and Theurkauf, 2010; Malone and Hannon, 2009; Siomi et al., 2010). In *Drosophila*, the primary piRNAs that initiate transposon silencing are derived from pericentromeric and subtelomeric chromatin domains composed of complex arrays of nested transposon fragments, termed piRNA clusters (Bergman et al., 2006; Brennecke et al., 2007). The *Drosophila flamenco* (*flam*) cluster, for example, spans approximately 180 kb of heterochromatin on the X chromosome (Brennecke et al., 2007; Mével-Ninio et al., 2007; Sarot et al., 2004). *P-element* insertion mutations at the 5′ end of this locus reduce expression of mature piRNAs and putative precursor transcripts from across the cluster and increase expression of the transposons represented by fragments in *flam* (Brennecke et al., 2007). piRNAs from *flam* are therefore proposed to transsilence homologous elements that are scattered throughout the genome.

The piRNA pool appears to be amplified by a ping-pong cleavage cycle in which antisense primary piRNAs from heterochromatic clusters, bound by the PIWI protein Aubergine (Aub), direct cleavage of transposon transcripts. This silences transposon expression and generates precursors for sense strand piRNAs that associate with Ago3. Ago3-piRNA complexes then cleave cluster transcripts to produce antisense piRNA precursors, completing the cycle (Brennecke et al., 2007; Gunawardane et al., 2007). Most of the proteins required for ping-pong amplification, including Ago3 and Aub, localize to the perinuclear nuage (Klattenhoff and Theurkauf, 2008; Lim and Kai, 2007; Malone et al., 2009). This germline-specific electron dense material is closely associated with the cytoplasmic face of nuclear pores (Eddy, 1974), but it is unclear how piRNA precursors are directed from clusters to the perinuclear-processing machinery. The DEAD box is a conserved ATP-dependent RNA binding motif (Linder and Jankowsky, 2011). The DEAD box protein Vasa (Vas) is required for germline development and piRNA production and was the first molecularly defined nuage component

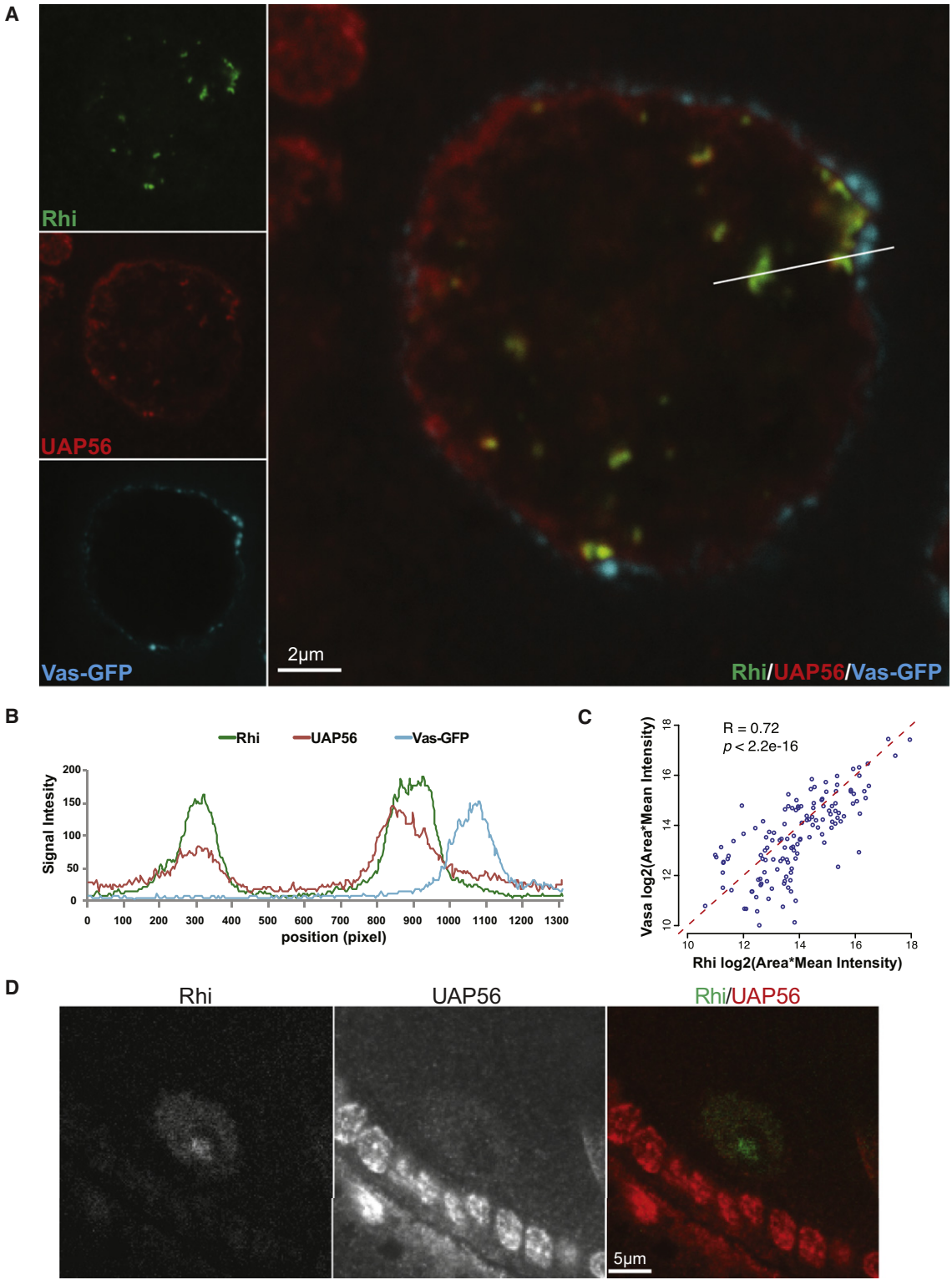

Figure 1. Organization of the piRNA Biogenesis Machinery

(A and B) UAP56, Rhi and Vasa localization in a stage 8 nurse cell. Single channel images are shown on left and a three-color merged image is show on the right (color assignments as indicated). The line in the merged image indicates the position of a line scan for fluorescence intensity (B). The nuclear foci contain overlapping peaks of UAP56 and Rhi, and Vasa-GFP signal accumulates across the nuclear envelope from foci that are closely associated with the periphery. Scale bars, 2 μm.

(Hay et al., 1990; Lasko and Ashburner, 1990; Liang et al., 1994; Malone et al., 2009). UAP56, by contrast, is a ubiquitously expressed DEAD box protein previously implicated in splicing and RNA export (Shen, 2009). Here we present evidence that UAP56 and Vas are cluster transcript binding proteins that organize a piRNA-processing compartment that spans the nuclear envelope.

RESULTS

UAP56 Colocalization with the piRNA Biogenesis Machinery

Drosophila piRNA pathway mutations lead to germline DNA damage and activation of a signaling cascade that blocks asymmetric RNA localization in the developing oocyte (reviewed by Khurana and Theurkauf, 2010). UAP56 has a conserved function in splicing and mRNA export, and strong hypomorphic mutations are lethal (Gatfield et al., 2001; MacMorris et al., 2003; Shen, 2009). However, *Drosophila* females carrying the *uap56$^{sz15'}$* allele (an E245K substitution) in *trans* to hypomorphic UTR deletions are sterile and show remarkably specific defects in asymmetric RNA localization (Eberl et al., 1997; Meignin and Davis, 2008), raising the possibility that UAP56 has a germline function in piRNA production and transposon silencing.

To explore a potential link to the piRNA pathway, we determined the subcellular localization of UAP56 relative to the piRNA-cluster-associated HP1 variant Rhino (Rhi) and the nuage component Vas (Figure 1). Immunofluorescence labeling and confocal imaging revealed UAP56 diffusely localized throughout germline and somatic nuclei but also concentrated in distinct nuclear foci in the nurse cells, which produce most of the maternal mRNAs that are deposited in the oocyte (Figure 1A). Strikingly, 98.4% of these foci, defined by UAP56 signal above background, colocalized with Rhi foci. Furthermore, 99.1% of Rhi signal above background colocalized with UAP56 foci (Figures 1A and 1B; Pearson's correlation coefficient R = 0.99). In the transcriptionally silent oocyte nucleus, however, Rhi localized to foci but UAP56 was dispersed (Figure 1D). In *rhi^{2}/rhi^{KG}* mutant ovaries, which do not express detectable Rhi protein, UAP56 was dispersed throughout the nucleus and did not form foci. Rhi is therefore required for UAP localization to nuclear foci, which may also require transcription.

We next assayed Rhi localization to nuclear foci in *uap56* mutants. The *uap56$^{sz15'}$* allele, when combined with hypomorphic 5′ UTR deletion alleles, is viable but sterile and leads to spindle class oocyte patterning defects that are characteristic of piRNA pathway mutations (Meignin and Davis, 2008). The point mutation in the *uap56$^{sz15'}$* allele does not alter protein expression (Meignin and Davis, 2008), and the *uap56^{28}* 5′ UTR deletion allele does not change protein structure but appears to reduce expression (Figure S2A available online; Meignin and Davis, 2008). The *uap56$^{sz15'}$/uap56^{28}* combination thus generates mutant ovaries in which most of the UAP56 is likely to carry the E245K substitution. In these ovaries, UAP56 was dispersed throughout the nurse cell nuclei. By contrast, Rhi was present in distinct foci during early oogenesis (Figure 2A). In later stage egg chambers, however, Rhi was dispersed in the nurse cell nuclei (Figure S2B). Low levels of wild-type UAP56, produced by the *uap56^{28}* allele, could support Rhi localization during early oogenesis. Alternatively, UAP56 could be required to maintain Rhi localization during later stages of oogenesis but dispensable for early localization. We favor the former possibility and speculate that UAP56 and Rhi are codependent for localization to nuclear foci.

To directly determine whether the E245K substitution alters the function and subcellular localization of UAP56, we generated transgenes expressing wild-type *uap56* (UAP56-Venus) or the *uap56$^{sz15'}$* mutant allele (sz-Venus) fused to the fluorescent protein Venus. Both transgenes were driven by the *uap56* promoter and integrated into the same chromosomal location, and western blots showed that both fusion proteins were expressed at comparable levels (Figure S2A). The wild-type UAP56-Venus fusion rescued the lethality associated with both *uap56^{28}/Df* and *uap56$^{sz15'}$/Df* combinations, and 75% of the embryos produced by *uap56$^{sz15'}$/Df* females expressing this fusion showed normal dorsal ventral patterning, and a small fraction of these embryos hatched (Table S1). The failure to restore full fertility is likely due to the Venus fusion because a genomic fragment expressing untagged protein fully rescues the mutant phenotype (Meignin and Davis, 2008). By contrast, the sz-Venus fusion failed to rescue viability in either mutant background (Table S1). To assay fusion protein localization in the ovary, we expressed both transgenes in the viable *uap56$^{sz15'}$/uap56^{28}* transheterozygous background and labeled for Rhi. Wild-type UAP56-Venus precisely colocalized with Rhi foci in early egg chambers (Figure 2B), and this transgene rescued Rhi localization to foci during later stages (data not shown). By contrast, the sz-Venus fusion was dispersed in the germline nuclei, did not colocalize with Rhi (Figure 2B), and failed to rescue Rhi foci in late stage egg chambers. The E245K substitution thus disrupts UAP56 colocalization with Rhi and Rhi focus stability.

UAP56 Is Required for Nuage Localization of piRNA Pathway Proteins

Our subcellular localization studies also showed that prominent UAP56-Rhi foci were closely associated with the nuclear periphery and that nuage foci containing a functional GFP-Vasa fusion appeared to localize directly across the nuclear envelope (Figure 1A). Labeling for Rhi, Vas, and nucleoporins (Figure S1A) showed that the pores lie between the nuclear foci containing Rhi and the nuage foci containing Vasa and

(C) Scatterplot comparing Rhi signal in foci at the nuclear periphery with Vasa signal in adjacent nuage foci. The diagonal indicates identical signal levels. *R* is the Pearson correlation coefficient, and the p value is based on Pearson's product moment correlation coefficient and follows a t distribution. 135 pairs of foci from 25 nuclei were quantified.

(D) In the oocyte, Rhi localizes to nuclear foci but UAP56 does not colocalize with these foci. Rhi and UAP56 are shown separately on the left, and a merged image with Rhi in green and UAP56 in red is on the right. Scale bars, 5 μm.

Also see Figure S1.

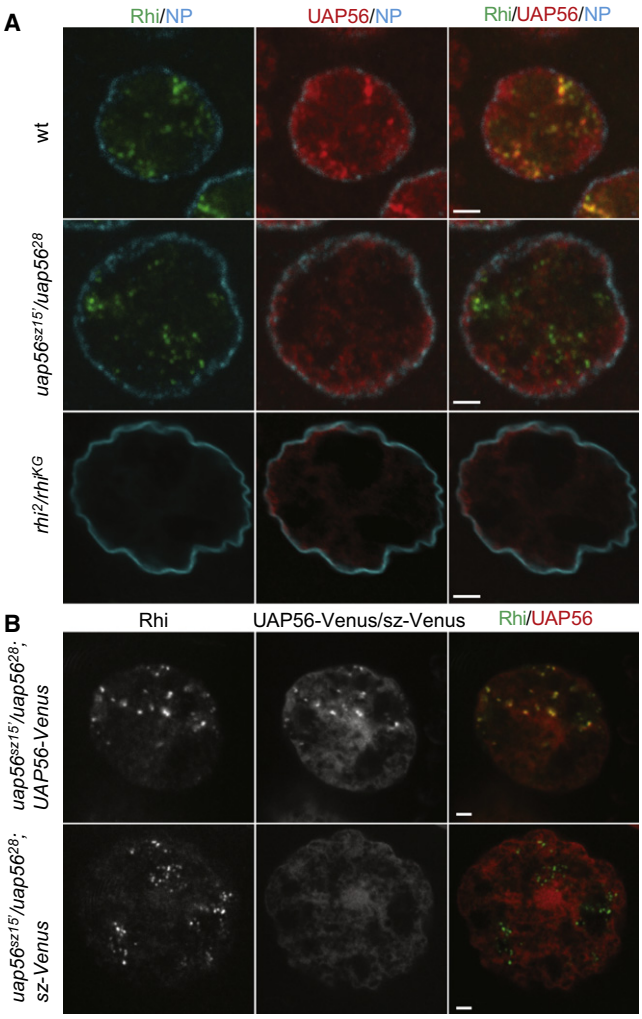

Figure 2. The E245K Substitution and *rhi* Mutations Disrupt UAP56 Localization to Nuclear Foci

(A) UAP56 (red), Rhi (green), and nuclear pores (cyan) in wild-type, *uap56*, and *rhi* mutant ovaries. UAP56 and Rhi are shown with nuclear pores (NP) in the first two images in each row. A merged image of Rhi, UAP56, and nuclear pores is show in the last panel of each row. In stage 4 $uap56^{sz15'}/uap56^{28}$ egg chambers, Rhi localizes to foci but UAP56 is dispersed in the nucleoplasm. In *rhi* mutations, Rhi protein is not detected, and UAP56 fails to localize to foci. Scale bars, 2 μm.

(B) Localization of transgenic wild-type UAP56-Venus and sz-Venus fusion proteins. Egg chambers expressing the transgenes were Immunolabeled for of Rhi (left, green on the right). Fusion protein distribution is show in the middle and in red on the right. sz-Venus, which carries the E245K substitution found in the $uap56^{sz15'}$ allele, fails to colocalize with Rhi foci. Scale bars, 2 μm.

Also see Figure S2 and Table S1.

that a significant fraction of Vasa signal overlaps with signal for the nuclear pores (Figure S1B). To quantify the relationship between Rhi foci in the nucleus and Vasa foci in nuage, we identified all Rhi foci that were above threshold and within the confocal resolution limit of nuclear pores (the signals overlapped) and, for each of these foci, determined if a focus of GFP-Vas was present at the adjacent nuclear periphery. A total of 98.5% of Rhi foci near the pores had an associated focus of Vasa at the cytoplasmic face of the nucleus. We then quantified Rhi in the nuclear foci and Vasa levels in the adjacent nuage foci. Strikingly, the level of Vas was highly correlated with the level of Rhi (Figure 1C; $R = 0.72$, $p < 2.2 \times 10^{-16}$). Furthermore, Vasa localization to nuage was disrupted in $uap56^{sz15'}/uap56^{28}$ mutants (Figure S3A). By contrast, and Rhi and UAP56 colocalized to distinct nuclear foci in *vas* mutants (Figure S2C). Rhi and UAP56 thus appear to function at clusters, in a process that is upstream of Vas localization to nuage.

The PIWI proteins Aub and Ago3 localize with Vas in nuage, where they appear to drive piRNA amplification. The founding member of the PIWI family, Piwi, is concentrated in nuclei (reviewed by Klattenhoff and Theurkauf, 2008). The $uap56^{sz15'}/uap56^{28}$ transheterozygous combination did not alter Piwi localization to nuclei but disrupted Aub and Ago3 localization to nuage (Figure 3A). Expression of wild-type UAP56-Venus in the $uap56^{sz15'}/uap56^{28}$ background partially restored nuage localization of Aub and fully restored nuage localization of Ago3 (Figure 3B). By contrast, transgenic expression of sz-Venus failed to restore nuage localization of either protein (Figure 3B). Aub and Vas localize to the posterior pole of the oocyte, where they are incorporated into pole plasm. Posterior localization of both proteins is disrupted in $uap56^{sz15'}/uap56^{28}$ mutants (Meignin and Davis, 2008) (Figures S3B and S3C). Posterior localization of Aub was restored in mutants expressing the wild-type UAP56-Venus transgene but not in mutants expressing the sz-Venus fusion (Figure S3C). We did not assay Vas localization in these transgenic ovaries, but Aub localization to pole plasm requires Vas (Harris and Macdonald, 2001), suggesting that Vas localization is also restored. The E245K substitution thus disrupts the organization of nuclear and cytoplasmic components of the piRNA biogenesis machinery.

Germline DNA Damage

piRNA pathway mutations lead to germline DNA damage, which is proposed to result from transposon mobilization (reviewed by Klattenhoff and Theurkauf, 2008). γH2Av is a phosphorylated histone variant that accumulates at DNA break sites (Madigan et al., 2002). In wild-type egg chambers, γH2Av foci are present in region 2 of the germarium, where meiotic breaks form, and in later nurse cell nuclei undergoing endoreduplication (Jang et al., 2003). Stage 2 and later oocyte nuclei, by contrast, are consistently negative for γH2Av foci. In $uap56^{sz15'}/uap56^{28}$ mutants, γH2Av foci persist in oocyte nuclei and appear to be enhanced in the nurse cells (Figure S4A). In $uap56^{sz15'}/uap56^{28}$ mutants expressing the wild-type UAP56-Venus transgene, by contrast, γH2Av foci were not detected in later stage oocytes (Figure S4A). UAP56 is therefore required to maintain germline genome integrity.

Gene and Transposon Expression

UAP56 is required for splicing and export of a broad spectrum of mRNAs (Gatfield et al., 2001; Shen, 2009) but our phenotypic and localization data raised the possibility that UAP56 also functions with Vas and Rhi to control transposon activity. We therefore used whole-genome tiling arrays to assay gene and transposon expression in $uap56^{sz15'}/uap56^{28}$ and *vas* mutant ovaries and compared these data with an earlier analysis of *rhi*

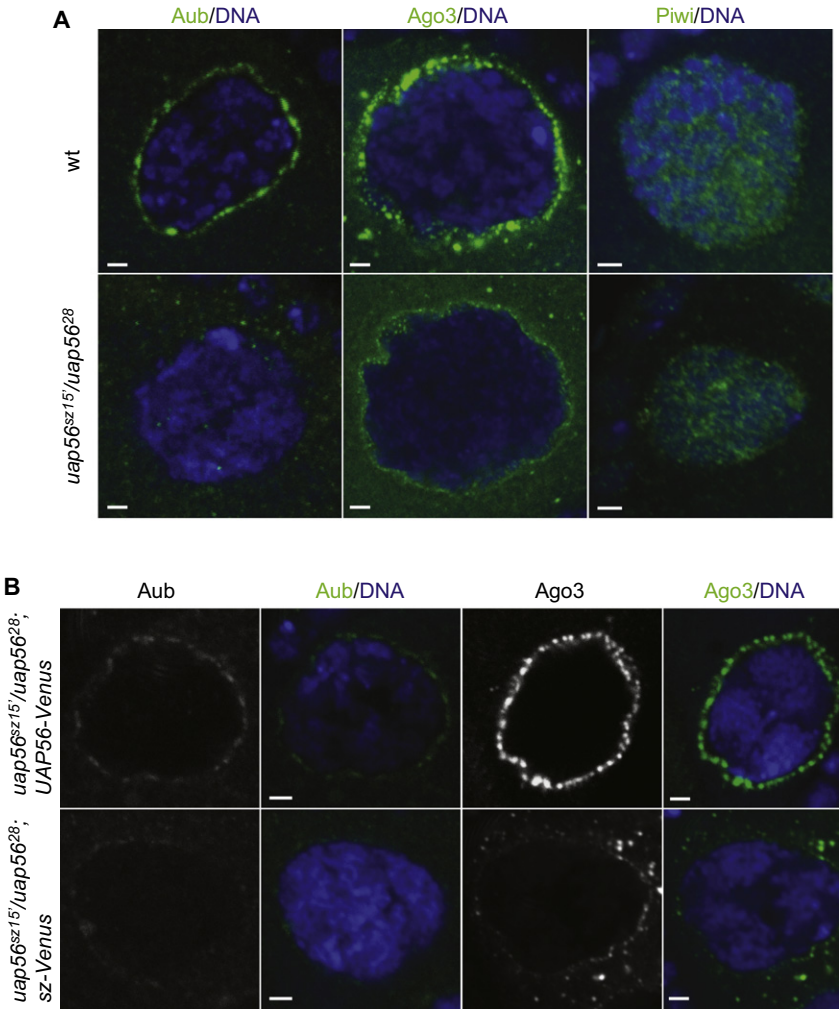

Figure 3. UAP56 Is Required for PIWI Protein Localization to Nuage

(A) Aub, Ago3, and Piwi localization in *Drosophila* nurse cells. Aub, Ago3, and Piwi are in green and DNA is in blue. Aub and Ago3 localized at perinuclear nuage in wild-type nurse cells, whereas Piwi is in nuclei of both nurse cells and follicle cells. In $uap56^{sz15'}/uap56^{28}$ mutants, Aub and Ago3 localization to nuage is disrupted, but Piwi localizes to the nucleus.

(B) Aub and Ago3 nuage localization is rescued by the wild-type UAP56-Venus transgene but not the not by the mutant sz-Venus transgene. Gray scale image shows Aub and Ago3 and merged images show Aub and Ago3 in green and DNA in blue. Scale bars, 2 μm.

Also see Figure S3.

mutants (Klattenhoff et al., 2009). The *vasa intronic gene (vig)* is contained in a *vas* intron, and Vig copurifies with FMRP and components of the siRNA machinery (Caudy et al., 2002), suggesting that it functions in RNA silencing. To specifically disrupt *vas*, we therefore analyzed a null deletion allele that removes both *vas* and *vig* in *trans* to a point mutation in *vas* that does not disrupt *vig.* The Genome Brower screen shot in Figure 4 shows expression of the retrotransposon *Blood* and neighboring *Ent1* gene, which contains three introns in control and *uap56*, *rhi*, and *vas* mutants. In all three mutants, *Blood* is overexpressed and *Ent1* is expressed at levels comparable to the control (Figure 4A). This pattern extends across the genome because no protein-coding gene showed a statistically significant difference from wild-type in *uap56*, *vas*, or *rhi* mutants (FDR < 0.05) (Figure 4C). By contrast, all three mutations disrupted transposon silencing, with 11 transposon families showing significant overexpression in *uap56*, *rhi*, and *vas* (FDR < 0.05; Figure 4B, red points; Venn diagram, Figure S4D). RT-qPCR and northern blotting confirmed that expression of a control protein coding gene (RP49) did not change and that two transposons (Het-A and Blood) were overexpressed (Figures S4B and S4C). The $uap56^{sz15'}/uap56^{28}$ allelic combination, and mutations in *vas* and *rhi*, thus disrupt transposon silencing but do not alter gene expression.

piRNA Production

To determine whether the $uap56^{sz15'}/uap56^{28}$ combination blocks production of piRNAs, we deeply sequenced small RNAs from mutant ovaries, which revealed a significant reduction in total piRNAs (Figures S5A and S5B). piRNAs from opposite strands that overlap by 10 nt are characteristic of ping-pong amplification. The bias toward 10 nt overlap was reduced in $uap56^{sz15'}/uap56^{28}$, *rhi*, and *vas* mutant ovaries (Figures S5C, S5D, and S5E). The scatterplots in Figure 5A show piRNAs mapping to group 1, 2, and 3 transposons in $uap56^{sz15'}/uap56^{28}$, *vas*, and *rhi* mutants compared with wild-type controls. In all three genotypes, piRNAs specific to group 1 transposable elements, which appear to be expressed primarily in the germline, are significantly reduced (Figure 5A, black points). By contrast, the levels of piRNAs linked to group 3 transposons, which are expressed primarily in the somatic follicle cells, were comparable to wild-type (Figure 5A, red points). Vas and Rhi both appear to be specific to the germline, consistent with changes in germline piRNAs. However, UAP56 is expressed in both the germline and somatic follicle cells. The $uap56^{28}/uap56^{sz15'}$ allelic combination thus appears to disrupt a germline-specific branch of the piRNA biogenesis pathway.

piRNA clusters that produce uniquely mapping piRNAs from both genomic strands dominate in the germline, whereas the major somatic piRNA cluster, *flam*, and cluster 2 produce unique piRNAs almost exclusively from one genomic strand (Brennecke et al., 2007; Gunawardane et al., 2007). Mutations in *rhi* nearly eliminate piRNAs from dual-strand clusters but do not block piRNA production by *flam* or cluster 2 (Klattenhoff et al., 2009). The $uap56^{28}/uap56^{sz15'}$ allelic combination

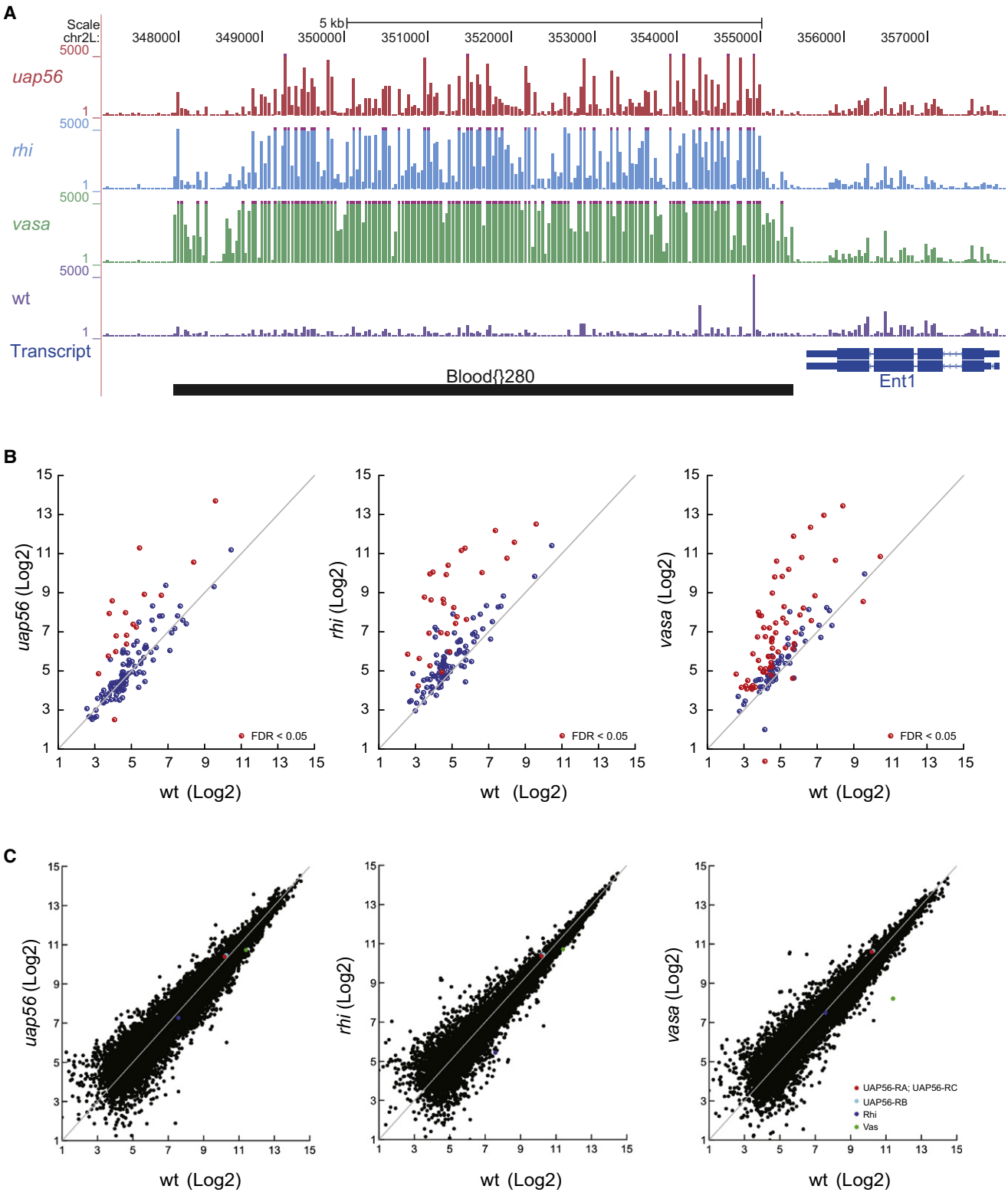

Figure 4. *uap56*, *rhi*, and *vasa* Mutations Disrupt Transposon Silencing but Do Not Alter Gene Expression

Whole-genome tiling arrays were used to assay gene and transposon expression in wild-type, $uap56^{sz15'}/uap56^{28}$, vas^{D5}/vas^{PH}, and $rhi^{02086}/rhi^{KG00910}$ ovaries. (A) A Genome Brower screen shot showing a region on chromosome 2L containing the nature transposon, Blood, and Ent1 gene. In *uap56*, *vas*, and *rhi* mutants, Blood expression is increased dramatically, whereas the Ent1 levels are comparable to control.

produces an essentially identical reduction in dual-strand-cluster expression (Figure 5B). Mutations in *vas* also block expression of dual-strand clusters and do not alter *flam* expression. However, *vas* mutations also reduce piRNAs linked to cluster 2, which appears to be expressed in the germline and soma (Figure 5B; (Malone et al., 2009). To directly compare cluster expression in the three mutant backgrounds, we generated pair-wise scatterplots covering the top 50 clusters (Figure 5C). This analysis showed that $uap56^{sz15'}/uap56^{28}$ and rhi^{2}/rhi^{KG} produce nearly identical changes in cluster expression (R = 0.96) and that very similar changes are produced by *vas* mutants (R = 0.83 for both *vas-uap56* and *vas-rhi* comparisons; Figure 5C). UAP56, Rhi and Vas thus represent nuclear and nuage components of a dual-strand-cluster expression system.

The majority of piRNAs in the *Drosophila* germline are derived from transposons and other repeats, but a subset map to gene transcripts. Chromosomal profiles of uniquely mapping 23 to 29 nt RNAs in $uap56^{sz15'}/uap56^{28}$ mutants revealed an increase in small RNAs from euchromatic sites (data not shown). Consistent with this observations, the scatterplots in Figure 5D show that 23 to 30 nt genic RNAs increase significantly in both *rhi* and *uap56* mutants. By contrast, *vas* produced a modest decrease in these genic RNAs. These data were normalized to sequencing depth, and reduced transposon mapping piRNAs could therefore artificially inflate the genic piRNA pool. We therefore normalized to total miRNAs and repeated the analysis, which confirmed the increase in genic 23 to 30 nt RNAs in *uap56* and *rhi* mutants (Figures S5I–S5K). Most of these species are derived from 3′ UTRs (Figure S5L). This 3′ UTR bias is also present in wild-type and *vas* mutants, but the high signal in *uap56* and *rhi* compresses profiles and obscures this bias.

In wild-type ovaries, genic small RNAs show a peak at 21 nt, which is characteristic of endo-siRNAs, and a peak at 26 nt, which is consistent with piRNAs bound to Piwi (Brennecke et al., 2007; Figure S5F). In $uap56^{sz15'}/uap56^{28}$ mutants, by contrast, the length distribution was much broader, with a shoulder between 20 and 22 nt (Figure S5G). Some of these species could be nonspecific mRNA breakdown products. Following binding to Piwi proteins, piRNAs are modified by the addition of a 2′-O-methyl group at the 3′ terminus (Horwich et al., 2007; Saito et al., 2007), which renders these species resistant to oxidation. To estimate the fraction of genic small RNAs that are bound to Piwi proteins, we therefore deep sequenced small RNAs after oxidation. These studies revealed a significant increase in oxidation-resistant genic small RNAs in *uap56* mutants, with a length distribution characteristic of Piwi binding (Figure S5H). Mutations in *uap56* thus reduce cluster piRNAs and increase genic piRNAs, suggesting that the specificity of processing has been compromised.

piRNA Precursor Binding

Clusters are proposed to produce long precursor RNAs that are processed into primary piRNAs in the nuage. Strand-specific RT-qPCR showed that the $uap56^{sz15'}/uap56^{28}$ combination significantly reduced the steady-state level of plus and minus strand RNAs from two regions of the major 42AB cluster (Figure S6A) but did not reduce precursor RNAs from unistrand cluster 2 or *flam* (Figure S6B). Mutations in *rhi* produce similar changes in cluster transcript abundance (Klattenhoff et al., 2009). DEAD box proteins can function as ATP-dependent RNA clamps (Linder and Jankowsky, 2011), and we speculated that UAP56 binds and stabilizes transcripts derived from germline clusters. To test this hypothesis, we immunoprecipitated wild-type UAP56-Venus and sz-Venus fusion proteins from ovary extracts and assayed RNA binding by random primed strand-specific deep sequencing. To quantify enrichment, genome mapping fragments in the input and precipitated fractions were normalized to noncoding RNAs (mainly ribosomal RNAs), which show only background binding to the beads.

Strikingly, RNAs from the major germline piRNA cluster at 42AB were the most highly enriched species in the UAP56-Venus precipitated fraction (34-fold: Figure 6 and Figure S6G, orange point), and piRNAs from 42AB are nearly eliminated by the *uap56* mutation (Figure 6). Transcripts from flanking protein coding gene show relatively modest enrichment, and transcripts from the somatic *flamenco* cluster were not enriched (Figure S6G, blue point). RT-qPCR confirmed that transcripts from cluster 1/42AB are enriched in the precipitated fraction, whereas transcripts from cluster 2, *flam* are not (Figure S6E). Across the transcriptome, RNAs from the top 40 piRNA producing clusters showed a 7.9-fold enrichment, and species from all 142 clusters identified by Brennecke et al. (2007) showed an average 5.2-fold enrichment. Protein coding genes, by contrast, showed no average enrichment (Figure S6H). The $uap56^{sz15'}$ mutation caused a modest, but statistically significant, reduction in RNA binding for both cluster transcripts and mRNAs (Figures 6A, S6E, S6G, and S6H). By contrast, this substitution does not significantly alter gene expression (Figure 4C) but nearly eliminates piRNA production by germline clusters (Figure 5B) and blocks UAP56 colocalization with Rhi (Figure 2). The E245K substitution thus appears to specifically block an interaction between UAP56 and the piRNA biogenesis machinery.

Primary piRNAs show a significant strand bias relative to the embedded transposon fragments that make up clusters, with 60% ± 24% accumulating antisense to the mobile elements (Brennecke et al., 2007). The longer RNAs that immunoprecipitate with UAP56, by contrast, do not show strand bias relative to the transposons (47% ± 23% antisense). For example, the region of the 42AB cluster composed of GATE transposon fragments in Figure 6B shows typical antisense piRNA strand bias but no clear bias in UAP56-bound RNAs. This difference in

(B) Scatterplots comparing the expression of transposons in mutants relative to wild-type. The diagonal indicates identical expression levels. All three mutants show significant (FDR < 0.05) overexpression of a subset of transposon families. Overexpression of selected transposon families was confirmed by northern blotting and qPCR (Figures S4B and S4C).

(C) Scatterplots comparing the expression of protein-coding genes in mutant and wild-type ovaries. None of the mutations lead to a significant change (FDR < 0.05) in protein coding genes expression. The *uap56*, *rhi*, and *vas* transcripts are highlighted, as indicated by the legend.

Also see Figure S4.

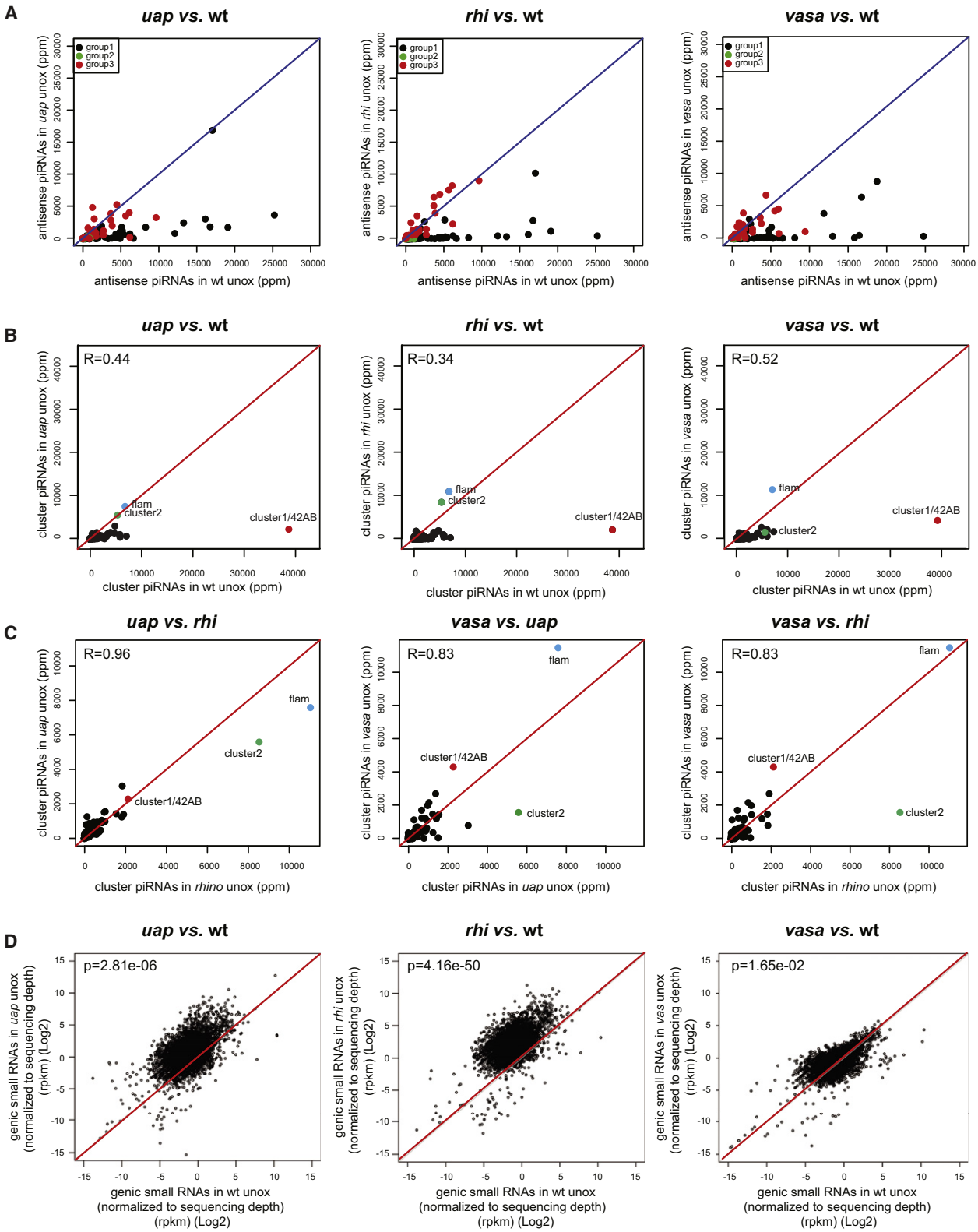

Figure 5. piRNA Expression in *uap56*, *rhi*, and *vasa* Mutant Ovaries

(A) Scatterplots comparing the abundance of piRNAs mapping to germline enriched group 1 transposons (black), soma enriched group 3 transposons (red),and class 2 transposons, which show a sense strand bias (green). All three mutations reduced piRNA from germline-specific group 1 transposon families.

strand bias is highly significant (p value = 1.123×10^{-6} by Wilcoxon signed rank test [paired]). Strand bias in the piRNA pool is proposed to originate from posttranscriptional ping-pong amplification of primary piRNAs (Brennecke et al., 2007). We therefore speculate that UAP56 binds to precursor RNAs that have not entered the piRNA amplification cycle.

The DEAD box protein Vas localizes across the nuclear envelope from UAP56 and is required for production of piRNAs from germline clusters. To determine whether cluster transcripts associate with Vas, we immunoprecipitated a functional Vas-GFP fusion from wild-type ovaries (Johnstone and Lasko, 2004) and assayed for cluster transcripts by RT-qPCR (Brennecke et al., 2007; Klattenhoff et al., 2009). Anti-GFP immunoprecipitation from the parental strain was used as a negative control. As shown in Figure S6F, RNAs from the 42AB cluster, but not from *flam* or unistrand cluster 2, were significantly enriched by Vas-GFP immunoprecipitation. The DEAD box is an ATP dependent RNA binding domain, suggesting that this interaction is direct. Steady-state cluster transcript levels were not reduced in *vas* mutants and may be somewhat elevated (Figures S6C and S6D). These observations suggest that Vas binds cluster transcripts as they exit the nucleus and deliver these RNAs to the piRNA biogenesis machinery.

The E245K Substitution Disrupts a Conserved Surface Residue

DEAD box proteins are composed of N- and C-terminal domains joined by a linker, and the ATP and RNA binding sites span these domains (reviewed by Linder and Jankowsky, 2011). In the ATP-bound "closed" state, these domains form an RNA clamp. The studies described here indicate that the E245K substitution in *uap56*$^{sz15'}$ defines a domain that is critical to piRNA production and transposon silencing. To define the location of this substitution on UAP56, we threaded the *Drosophila* sequence into the crystal structure of the ATP bound form of human UAP56 (Shi et al., 2004; Zhao et al., 2004). This modeling places E245 at the protein surface, near the linker between the two UAP56 domains (Figure 7A). This residue appears to form a salt bridge between the end of an α-helix and β sheet, and a structurally analogous salt bridge appears to stabilize the closed ATP and RNA binding conformation in the related DEAD box protein Dpb5(Montpetit et al., 2011). This bridge is disrupted in the open form, which is engaged with the nuclear pore and the Gle1 activator and does not bind RNA (Montpetit et al., 2011). The E245K substitution in *uap56*$^{sz15'}$ may therefore contribute to the observed reduction in mRNA and cluster transcript binding (Figures S6E, S6G, and S6H). By contrast, this substitution nearly eliminates piRNA production and colocalization with Rhi but does not disrupt steady-state mRNA expression (Figures 2, 4C, and 5B). Reduced RNA binding cannot explain this specificity. We therefore propose that this surface residue lies in a domain of UAP56 that interacts with the piRNA machinery but is dispensable for mRNA export and processing. This residue is conserved from humans to fission yeast (Figure S7), raising the possibility that this domain mediates interactions with the small RNA silencing machinery in other systems.

DISCUSSION

piRNAs potently repress transposon activity during germline development and thus play a critical role in maintaining the inherited genome complement (Malone and Hannon, 2009; Siomi et al., 2010). Heterochromatic clusters encode primary piRNAs, but most of the piRNA biogenesis machinery is concentrated in the perinuclear nuage, which is closely associated with the cytoplasmic face of nuclear pores (Eddy, 1974, 1975; Klattenhoff and Theurkauf, 2008; Lim and Kai, 2007). How transcripts are directed from clusters to the perinuclear piRNA biogenesis machinery, and how gene transcripts are excluded from this machinery, are not understood. We show that the DEAD box protein UAP56 colocalizes with the cluster-associated HP1 homolog Rhi and that prominent foci containing both Rhi and UAP56 are closely associated with the nuclear periphery, directly opposite nuage foci containing Vas (Figure 1A). Strikingly, an E245K mutation that prevents UAP56 colocalization with Rhi (Figure 2) also disrupts nuage localization of piRNA biogenesis proteins (Figure 3), transposon silencing (Figure 4), and piRNA production by the dual-strand clusters (Figures 5 and S5). This mutation also increases ectopic piRNAs from protein coding genes (Figure 5D). UAP56 thus has a previously unrecognized role in germline piRNA biogenesis and transposon silencing. Intriguingly, studies in *Caenorhabditis elegans* indicate that Vas-containing p-granules, which appear to be equivalent to nuage, form a size exclusion zone that extends the nuclear pore (Updike et al., 2011). We therefore propose that UAP56 functions with Vas to organize a piRNA-processing compartment that spans the nuclear pore and increases the efficiency and specificity of piRNA production by coordinately directing cluster transcripts to processing factors in the nuage and excluding gene transcripts from these factors (Figure 7B).

DEAD box proteins appear to function as ATP-dependent RNA clamps(Linder and Jankowsky, 2011), and transcripts from the major dual-strand cluster immunoprecipitate with both UAP56 and Vas (Figures S6E and S6F). Intriguingly, UAP56 and Vas are closely associated with opposite faces of nuclear pore complexes (Figures 1 and S1), and nucleoporins stimulate ATP

(B) Scatterplots comparing the abundance of cluster piRNAs in three mutants and wild-type ovaries. Each point represents piRNAs from a single cluster. All three mutations significantly reduced piRNAs to the germline clusters, including the major dual-strand cluster at 42AB (red). By contrast, *uap56* and *rhi* mutants do not reduced piRNA to unistrand cluster 2 (green) or *flam* (blue). Mutations in *vas*, but not *flam*, reduce piRNAs linked to cluster 2.

(C) Pair-wise comparison of cluster piRNAs in mutant ovaries. Cluster expression is highly correlated in all three mutants, and *rhi* and *uap56* show almost identical patterns of cluster piRNA expression (R = 0.96).

(D) Genic piRNA expression in mutant ovaries. Scatterplots compare the abundance of piRNAs linked to protein coding genes in mutant ovaries relative to wild-type controls. Both *uap56* and *rhi* mutants lead to a significant increase in ectopic piRNAs from protein coding genes. R values are shown at upper left corner. RNA sequencing data for *vas* and *rhi* are from Malone et al. (2009) and Klattenhoff et al. (2009).

Also see Figure S5.

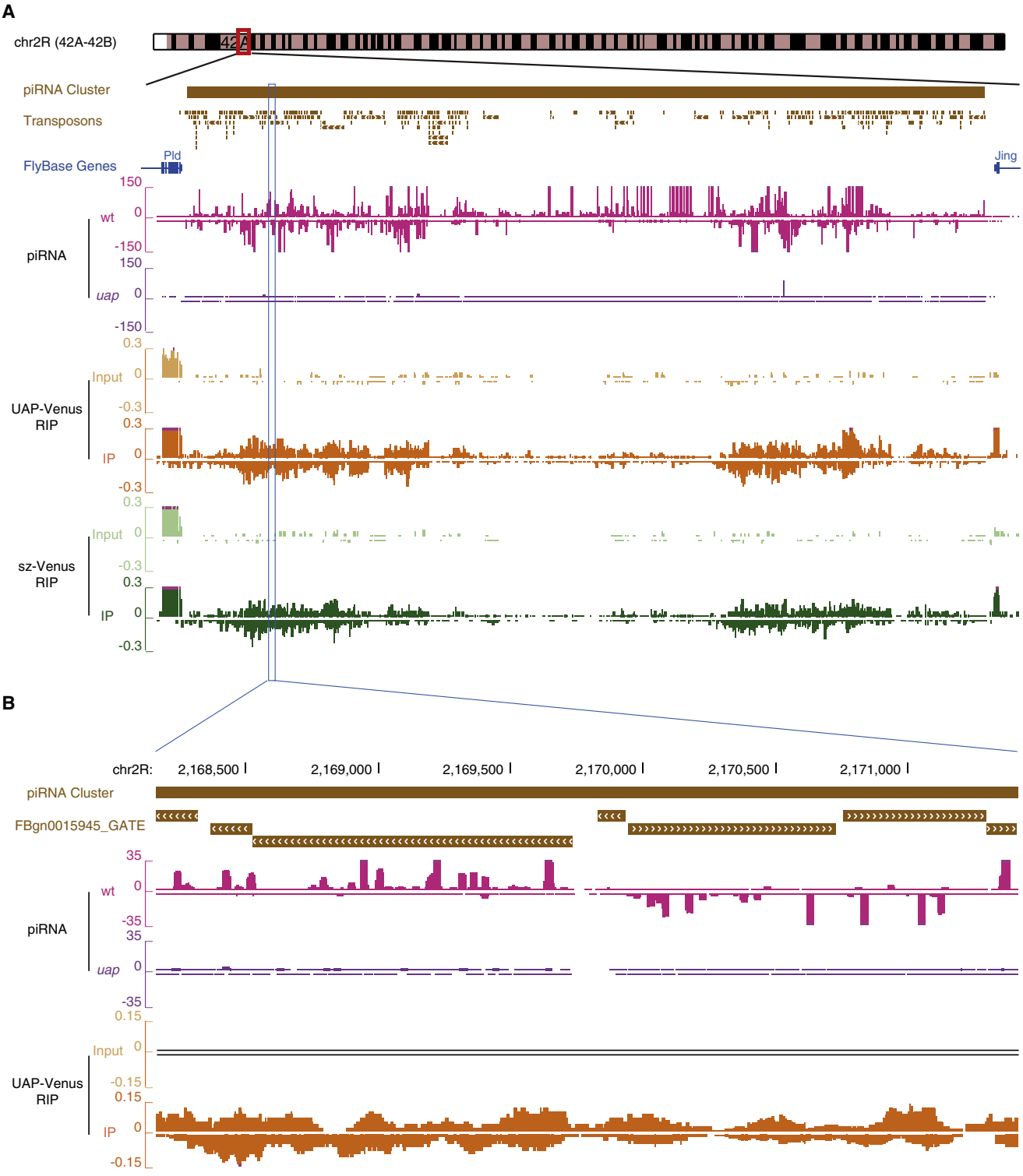

Figure 6. piRNA Expression and Precursor Binding to UAP56

(A) piRNAs and UAP56-associated RNAs mapping to the 1/42AB on chromosome 2R. The locus has many embedded transposable elements and is flanked by protein coding genes Pld and Jing. In wild-type, piRNAs map to both the plus and minus strands of the 42AB cluster (pink tracks) and are dramatically reduced in *uap56*$^{sz15'}$/*uap56*^{28} mutants (purple tracks). Wild-type UAP56-Venus and sz-Venus transgenes were expressed in *w*^{1} ovaries and immunoprecipitated with anti-FLAG. Bound RNAs were quantified by strand-specific RNA-Seq. The UAP-Venus input signal is in light brown, the UAP-Venus IP signal is in orange, the sz-Venus input is in light green, and the sz-Venus IP signal is in dark green. All signals are normalized to ribosomal RNAs. Cluster transcripts were highly enriched over input

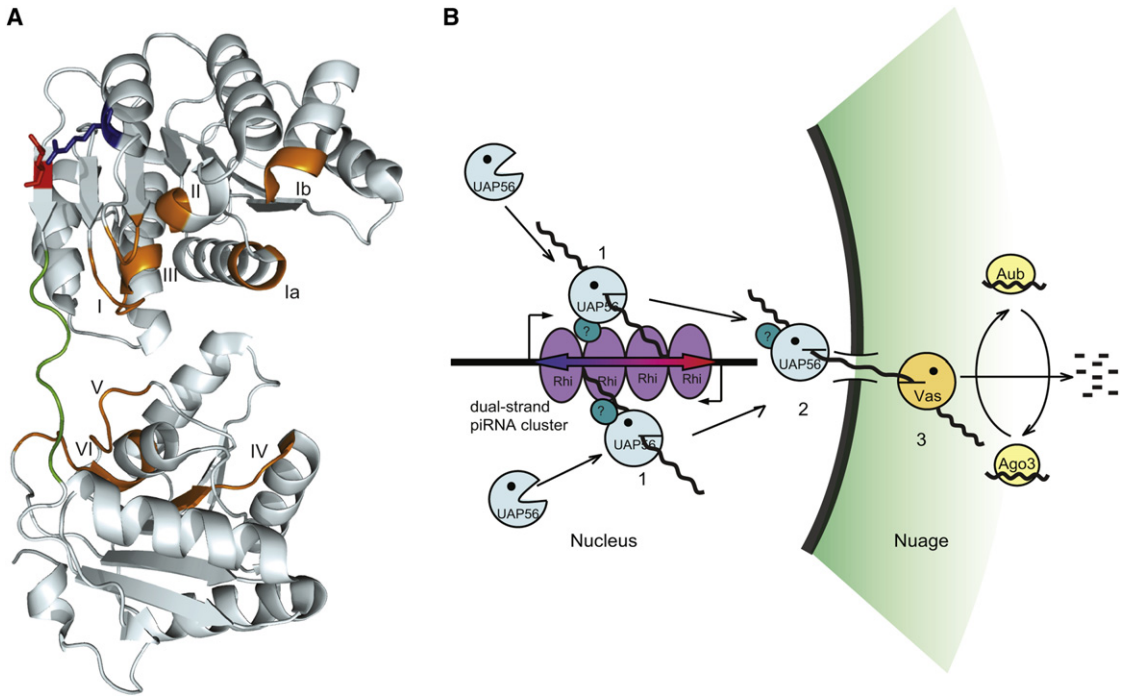

Figure 7. UAP56 Structure and Function in a piRNA-Processing Compartment

(A) *Drosophila* UAP56 amino acid sequence treaded into a high-resolution crystal structure of human UAP56. The N-terminal and C-terminal domains are connected by a flexible linker (green), and ATP and RNA binding motifs (orange) are located at the interface between the two domains. Glutamate 245 (red), which is changed to a lysine in *uap56sz*$^{15'}$, is located in a β sheet in the N-terminal domain that is attached to the linker. This negatively charged residue also appears to form a salt bridge with Arg236 (blue), which is located in an α-helix in the N-terminal domain.

(B) A model for UAP56 function within piRNA-processing compartment that spans the nuclear envelope. (1) UAP56 associates with nascent transcripts from dual-strand piRNA clusters, which bind the HP1 homolog Rhi. We speculate that UAP56 interacts with clusters through a domain defined by residue 245E. (2) UAP56-cluster transcript complexes interact with the nuclear pore, which triggers RNA release and export. (3) Vas binds cluster transcripts within the pore, or as they emerge from the pore and enter nuage, and then delivers these RNAs to the processing machinery.

Also see Figure S7.

hydrolysis and RNA release by related DEAD box proteins (Montpetit et al., 2011). UAP56 binding to nuclear pores could therefore trigger release of cluster transcripts, which are bound by the DEAD box protein Vas in the nuage. We speculate that Vas directs these RNAs to the primary piRNA-processing machinery and to Aub, which binds primary piRNAs and copurifies with Vas (Lim and Kai, 2007; Malone et al., 2009).

The majority of piRNA pathway proteins are germline specific, but UAP56 is an ubiquitously expressed essential gene. The *uap56*$^{sz15'}$ allele thus reveals a link between germline-specific piRNA pathway components and the general RNA splicing and export machinery. It is interesting to note that mutations in the *Drosophila mago nashi* and *tsunagi/Y14* genes, which encode conserved exon junction components, lead to axis specification defects that are strikingly similar to the defects associated with the *uap56*$^{sz15'}$ allele and other piRNA pathway mutants (Micklem et al., 1997; Mohr et al., 2001; Newmark and Boswell, 1994; Newmark et al., 1997). This may reflect a function for the splice junction complex, with UAP56, in piRNA production and transposon silencing.

EXPERIMENTAL PROCEDURES

Fly Stocks and Transgenic Lines

All the stocks and crosses were raised at 25° C on cornmeal medium and with standard conditions. OregonR (OreR) and *w*^{1118} were used as control strains. The *uap56*$^{sz15'}$*/CyO*, *uap56*^{28}*/CyO* and UASp-UAP56-GFP stocks were obtained from Ilan Davis (University of Oxford). *uap56*^{Df}*/CyO*, *vas*^{D5}*/CyO*, *vas*^{PH}*/CyO*, *rhi*^{2} (*rhi*^{02086})*/CyO*, and *rhi*^{KG} (*rhi*^{KG00910})*/CyO* were obtained from Bloomington Stock Center.

The UASp-UAP56-GFP transgene was constructed by using a full-length UAP56 cDNA from the Gold collection (BDGP23644). Coding sequences were recovered by PCR amplification with a sense primer (5′-GGTACCATGG

by both wild-type UAP56-Venus and sz-Venus IP immunoprecipitation. By contrast, the neighboring gene, Pld, showed a modest enrichment. The sz-Venus mutant showed somewhat diminished enrichment relative to wild-type, for both cluster and gene transcripts.

(B) Cluster-specific piRNAs (pink) accumulate antisense to the embedded transposon fragments (brown, direction of transcription indicated by arrowheads). UAP56 bound precursor RNAs are derived from the same regions, but do not show clear strand bias (UAP-Venus RIP).

Also see Figure S6.

CCGACAATGACGATC-3′) that spanned the translation initiation codon, and an antisense primer that introduced a unique Nhe1 restriction site upstream of the stop codon (5′-GCTAGCGCGTCCCTCAATGAATGTAG-3′). The PCR product was cloned into pGemT (Promega) and sequenced. Two silent mutations at position 22 (GAA to GAG) and 87 (TCC to TCT) of the protein were detected. The UAP56 cDNA was fused to the N terminus of GFP (from vector KS-GFP kindly provided by A. Vincent). A KpnI-BamHI fragment encoding the UAP56-GFP fusion was cloned downstream of the promoter in the UASp transformation vector (Rørth, 1998). Transgenic lines were obtained in *w1* background, and transgene expression was induced by using the germline-specific nanos Gal4 vp16 driver.

The UAP56-Venus transgene was engineered as follows: The UAP56 promoter and 5′ UTR (695bp) were cloned upstream of a full-length cDNA, which was fused in frame to a multifunction affinity purification tag followed by Venus. (Ma et al., 2012). The fusion was followed by *uap56* 3′ UTR (1255bp). Site directed mutagenesis was used to generate a G to A substitution at position 733 of the *uap56* coding sequence, producing the E245K substitution found in the $uap56^{sz15'}$ allele. The wild-type and $uap56^{sz15'}$ fusion genes were introduced into the attB vector, and independent transformants were obtained by site-direct phiC31 integration into chromosomal locus 68A4 (Ni et al., 2008).

Immunohistochemistry

Ovaries were immunolabeled by using the Buffer A staining protocol, as described earlier (Klattenhoff et al., 2009). The following primary antibodies and dilutions were used: rabbit anti-Aub (1:1000)(Brennecke et al., 2007), rabbit anti-Ago3 (1:250)(Li et al., 2009), rabbit anti-Piwi (1:1000), rabbit anti-UAP56 (1:1,000)(Eberl et al., 1997), guinea pig anti-Rhi (1:500)(Klattenhoff et al., 2009), and rabbit anti-Vas (1:5,000)(Liang et al., 1994). Anti-UAP56 and anti-Vas were gifts from P. Lasko. A rabbit polyclonal antibody against γ-H2Av (1:500, Rockland) was used to detect DNA DSBs. A mouse monoclonal antibody against nuclear pore complex (1:1,000, Covance) was used to label nuclear envelope. TOTO-3 dye (Molecular Probes) was used at 1:500 to label DNA after RNase One (1:500, Promega) treatment.

Total RNA Isolation and Array Analyses

Total RNA was extracted from 2- to 4-day-old ovaries from OreR, $uap56^{sz15'}$/$uap56^{28}$, rhi^{2}/rhi^{KG}, and vas^{D5}/vas^{PH} females by using the RNeasy Kit (QIAGEN) and the manufacturer's instructions. Tilling array analysis was performed as described previously (Klattenhoff et al., 2009). Data can be accessed through GEO reference series GSE35638.

Small RNA Sequencing

Total RNA was extracted from ovaries dissected from 2- to 4-day-old females by using MirVana kit (Ambion). A totatl of 18–29 nt small RNAs were gel purified following 2S rRNA depletion and libraries were prepared as described previously (Klattenhoff et al., 2009). Sequencing was performed with a Solexa Genome Analyzer (Illumina).

Small RNA sequence analysis was performed as described previously(Klattenhoff et al., 2009; Li et al., 2009). Data can be accessed through GEO reference series GSE35638.

Strand-Specific Reverse Transcriptase qPCR

Strand-specific RT-qPCR for cluster transcripts was performed as described previously (Klattenhoff et al., 2009). Signals were normalized to 18 s rRNA after subtracting no RT primer background.

RNA Immunoprecipitation and Strand-Specific RNA Sequencing

Whole ovaries were dissected from 2- to 4-day-old flies in 1 × PBS Buffer and homogenized on ice in Lysis Buffer (50 mM Tris-HCl, pH 7.5, 150 mM NaCl, 1 mM EDTA, 0.5% NP-40) with 40 U/ml RNasin Plus (Promega N261), 1 × Proteinase Inhibitor Cocktail (Sigma) and 1 mM PMSF. The lysate was sonicated three times for 5 s each at 35% amplitude with a Diagenode Bioruptor, and then centrifuged at 14,000rpm for 15 min at 4°C in a table top microfuge. 10% of the supernatants were saved as input samples and the rest were incubated with GFP Trap-A beads (Chromotek) for 2 hr at 4°C. The beads were separated from the supernatants after incubation and washed three times with Lysis Buffer at room temperature. UAP56-Venus and sz-Venus were immunoprecipitated by ANTI-FLAG M2 Affinity Gel (Sigma A2220) and eluted with 200 μg/ml FLAG Peptide (Sigma F3290). Three biological replicates were performed for each IP. Total RNA was extracted from the input lysate and the beads by using RNeasy Micro Kit (QIAGEN) according to the manufacturer's protocol. Strand-specific RNA sequencing was performed after depletion of ribosomal RNAs with Ribo-Zero (Epicenter Inc) by a modification of the procedure of Parkhomchuk et al. (Parkhomchuk et al., 2009), described in detail elsewhere (Z.Z. and P.D.Z., unpublished data). Data can be accessed through GEO reference series GSE35638.

Quantification of Transposon Transcripts Levels by RT-qPCR

Total RNA was prepared from whole ovaries with RNeasy Mini Kit (QIAGEN#74104). $Oligo(dT)_{20}$ primer was mixed with an 18 s rRNA-specific control primer and first strand cDNAs were synthesized with SuperScriptIII reverse transcriptase (Invitrogen, 18080-093) following the manufacture's protocol. The resulting cDNAs were used as templates for quantitative real-time PCR with the primers indicated (Table S2). qPCR reactions were performed by using a StepOnePlus System (Applied Biosystems) and SYBR Green I (QIAGEN, 204145). The expression level of transcripts was measured relative to the 18 s rRNA internal control. Background obtained with no RT primer reactions was subtracted. Three technical replicates were performed for each RT primer. Graphs show the average and SD.

Other Procedures

Western blots were quantified by using an Odyssey Infrared Imaging System (LI-COR). Rabbit polyclonal anti-UAP56 antibody was used as 1:1,000, and the mouse monoclonal anti-actin antibody (DSHB, JLA20) was used as 1:20. Northern blots were performed as described previously (Klattenhoff et al., 2007).

ACCESSION NUMBERS

The GEO accession number for the reference series reported in this paper is GSE35638.

SUPPLEMENTAL INFORMATION

Supplemental Information includes Extended Experimental Procedures, seven figures, and two tables and can be found with this article online at http://dx.doi.org/10.1016/j.cell.2012.09.040.

ACKNOWLEDGMENTS

Thanks to members of the Theurkauf and Weng labs for critical discussions and constructive criticisms, to Dr. Paul Lasko for antibodies, and to the Bloomington Drosophila Stock Center for strains. Special thanks to Melissa Moore for sharing her insights into DEAD box proteins. This work was supported by NIH grant HD049116.

Received: December 1, 2011
Revised: March 9, 2012
Accepted: September 20, 2012
Published: November 8, 2012

REFERENCES

Aravin, A.A., Hannon, G.J., and Brennecke, J. (2007). The Piwi-piRNA pathway provides an adaptive defense in the transposon arms race. Science *318*, 761–764.

Bennetzen, J.L. (2000). Transposable element contributions to plant gene and genome evolution. Plant Mol. Biol. *42*, 251–269.

Bergman, C.M., Quesneville, H., Anxolabéhère, D., and Ashburner, M. (2006). Recurrent insertion and duplication generate networks of transposable element sequences in the Drosophila melanogaster genome. Genome Biol. *7*, R112.

Brennecke, J., Aravin, A.A., Stark, A., Dus, M., Kellis, M., Sachidanandam, R., and Hannon, G.J. (2007). Discrete small RNA-generating loci as master regulators of transposon activity in Drosophila. Cell *128*, 1089–1103.

Britten, R.J. (2010). Transposable element insertions have strongly affected human evolution. Proc. Natl. Acad. Sci. USA *107*, 19945–19948.

Caudy, A.A., Myers, M., Hannon, G.J., and Hammond, S.M. (2002). Fragile X-related protein and VIG associate with the RNA interference machinery. Genes Dev. *16*, 2491–2496.

Eberl, D.F., Lorenz, L.J., Melnick, M.B., Sood, V., Lasko, P., and Perrimon, N. (1997). A new enhancer of position-effect variegation in Drosophila melanogaster encodes a putative RNA helicase that binds chromosomes and is regulated by the cell cycle. Genetics *146*, 951–963.

Eddy, E.M. (1974). Fine structural observations on the form and distribution of nuage in germ cells of the rat. Anat. Rec. *178*, 731–757.

Eddy, E.M. (1975). Germ plasm and the differentiation of the germ cell line. Int. Rev. Cytol. *43*, 229–280.

Gatfield, D., Le Hir, H., Schmitt, C., Braun, I.C., Köcher, T., Wilm, M., and Izaurralde, E. (2001). The DExH/D box protein HEL/UAP56 is essential for mRNA nuclear export in Drosophila. Curr. Biol. *11*, 1716–1721.

Ghildiyal, M., and Zamore, P.D. (2009). Small silencing RNAs: an expanding universe. Nat. Rev. Genet. *10*, 94–108.

Gunawardane, L.S., Saito, K., Nishida, K.M., Miyoshi, K., Kawamura, Y., Nagami, T., Siomi, H., and Siomi, M.C. (2007). A slicer-mediated mechanism for repeat-associated siRNA 5′ end formation in Drosophila. Science *315*, 1587–1590.

Harris, A.N., and Macdonald, P.M. (2001). Aubergine encodes a Drosophila polar granule component required for pole cell formation and related to eIF2C. Development *128*, 2823–2832.

Hay, B., Jan, L.Y., and Jan, Y.N. (1990). Localization of vasa, a component of Drosophila polar granules, in maternal-effect mutants that alter embryonic anteroposterior polarity. Development *109*, 425–433.

Hedges, D.J., and Belancio, V.P. (2011). Restless genomes humans as a model organism for understanding host-retrotransposable element dynamics. Adv. Genet. *73*, 219–262.

Horwich, M.D., Li, C., Matranga, C., Vagin, V., Farley, G., Wang, P., and Zamore, P.D. (2007). The Drosophila RNA methyltransferase, DmHen1, modifies germline piRNAs and single-stranded siRNAs in RISC. Curr. Biol. *17*, 1265–1272.

Jang, J.K., Sherizen, D.E., Bhagat, R., Manheim, E.A., and McKim, K.S. (2003). Relationship of DNA double-strand breaks to synapsis in Drosophila. J. Cell Sci. *116*, 3069–3077.

Johnstone, O., and Lasko, P. (2004). Interaction with eIF5B is essential for Vasa function during development. Development *131*, 4167–4178.

Khurana, J.S., and Theurkauf, W. (2010). piRNAs, transposon silencing, and Drosophila germline development. J. Cell Biol. *191*, 905–913.

Klattenhoff, C., and Theurkauf, W. (2008). Biogenesis and germline functions of piRNAs. Development *135*, 3–9.

Klattenhoff, C., Bratu, D.P., McGinnis-Schultz, N., Koppetsch, B.S., Cook, H.A., and Theurkauf, W.E. (2007). Drosophila rasiRNA pathway mutations disrupt embryonic axis specification through activation of an ATR/Chk2 DNA damage response. Dev. Cell *12*, 45–55.

Klattenhoff, C., Xi, H., Li, C., Lee, S., Xu, J., Khurana, J.S., Zhang, F., Schultz, N., Koppetsch, B.S., Nowosielska, A., et al. (2009). The Drosophila HP1 homolog Rhino is required for transposon silencing and piRNA production by dual-strand clusters. Cell *138*, 1137–1149.

Lasko, P.F., and Ashburner, M. (1990). Posterior localization of vasa protein correlates with, but is not sufficient for, pole cell development. Genes Dev. *4*, 905–921.

Li, C., Vagin, V.V., Lee, S., Xu, J., Ma, S., Xi, H., Seitz, H., Horwich, M.D., Syrzycka, M., Honda, B.M., et al. (2009). Collapse of germline piRNAs in the absence of Argonaute3 reveals somatic piRNAs in flies. Cell *137*, 509–521.

Liang, L., Diehl-Jones, W., and Lasko, P. (1994). Localization of vasa protein to the Drosophila pole plasm is independent of its RNA-binding and helicase activities. Development *120*, 1201–1211.

Lim, A.K., and Kai, T. (2007). Unique germ-line organelle, nuage, functions to repress selfish genetic elements in Drosophila melanogaster. Proc. Natl. Acad. Sci. USA *104*, 6714–6719.

Linder, P., and Jankowsky, E. (2011). From unwinding to clamping - the DEAD box RNA helicase family. Nat. Rev. Mol. Cell Biol. *12*, 505–516.

Ma, H., McLean, J.R., Chao, L.F., Mana-Capelli, S., Paramasivam, M., Hagstrom, K.A., Gould, K.L., and McCollum, D. (2012). A highly efficient multifunctional tandem affinity purification approach applicable to diverse organisms. Mol. Cell. Proteomics *11*, 501–511.

MacMorris, M., Brocker, C., and Blumenthal, T. (2003). UAP56 levels affect viability and mRNA export in Caenorhabditis elegans. RNA *9*, 847–857.

Madigan, J.P., Chotkowski, H.L., and Glaser, R.L. (2002). DNA double-strand break-induced phosphorylation of Drosophila histone variant H2Av helps prevent radiation-induced apoptosis. Nucleic Acids Res. *30*, 3698–3705.

Malone, C.D., and Hannon, G.J. (2009). Small RNAs as guardians of the genome. Cell *136*, 656–668.

Malone, C.D., Brennecke, J., Dus, M., Stark, A., McCombie, W.R., Sachidanandam, R., and Hannon, G.J. (2009). Specialized piRNA pathways act in germline and somatic tissues of the Drosophila ovary. Cell *137*, 522–535.

Meignin, C., and Davis, I. (2008). UAP56 RNA helicase is required for axis specification and cytoplasmic mRNA localization in Drosophila. Dev. Biol. *315*, 89–98.

Mével-Ninio, M., Pelisson, A., Kinder, J., Campos, A.R., and Bucheton, A. (2007). The flamenco locus controls the gypsy and ZAM retroviruses and is required for Drosophila oogenesis. Genetics *175*, 1615–1624.

Micklem, D.R., Dasgupta, R., Elliott, H., Gergely, F., Davidson, C., Brand, A., González-Reyes, A., and St Johnston, D. (1997). The mago nashi gene is required for the polarisation of the oocyte and the formation of perpendicular axes in Drosophila. Curr. Biol. *7*, 468–478.

Mohr, S.E., Dillon, S.T., and Boswell, R.E. (2001). The RNA-binding protein Tsunagi interacts with Mago Nashi to establish polarity and localize oskar mRNA during Drosophila oogenesis. Genes Dev. *15*, 2886–2899.

Montpetit, B., Thomsen, N.D., Helmke, K.J., Seeliger, M.A., Berger, J.M., and Weis, K. (2011). A conserved mechanism of DEAD-box ATPase activation by nucleoporins and InsP6 in mRNA export. Nature *472*, 238–242.

Newmark, P.A., and Boswell, R.E. (1994). The mago nashi locus encodes an essential product required for germ plasm assembly in Drosophila. Development *120*, 1303–1313.

Newmark, P.A., Mohr, S.E., Gong, L., and Boswell, R.E. (1997). mago nashi mediates the posterior follicle cell-to-oocyte signal to organize axis formation in Drosophila. Development *124*, 3197–3207.

Ni, J.Q., Markstein, M., Binari, R., Pfeiffer, B., Liu, L.P., Villalta, C., Booker, M., Perkins, L., and Perrimon, N. (2008). Vector and parameters for targeted transgenic RNA interference in Drosophila melanogaster. Nat. Methods *5*, 49–51.

Parkhomchuk, D., Borodina, T., Amstislavskiy, V., Banaru, M., Hallen, L., Krobitsch, S., Lehrach, H., and Soldatov, A. (2009). Transcriptome analysis by strand-specific sequencing of complementary DNA. Nucleic Acids Res. *37*, e123.

Rørth, P. (1998). Gal4 in the Drosophila female germline. Mech. Dev. *78*, 113–118.

Saito, K., Sakaguchi, Y., Suzuki, T., Suzuki, T., Siomi, H., and Siomi, M.C. (2007). Pimet, the Drosophila homolog of HEN1, mediates 2′-O-methylation of Piwi- interacting RNAs at their 3′ ends. Genes Dev. *21*, 1603–1608.

Sarot, E., Payen-Groschêne, G., Bucheton, A., and Pélisson, A. (2004). Evidence for a piwi-dependent RNA silencing of the gypsy endogenous retrovirus by the Drosophila melanogaster flamenco gene. Genetics *166*, 1313–1321.

Shen, H. (2009). UAP56- a key player with surprisingly diverse roles in pre-mRNA splicing and nuclear export. BMB Rep *42*, 185–188.

Shi, H., Cordin, O., Minder, C.M., Linder, P., and Xu, R.M. (2004). Crystal structure of the human ATP-dependent splicing and export factor UAP56. Proc. Natl. Acad. Sci. USA *101*, 17628–17633.

Siomi, M.C., Miyoshi, T., and Siomi, H. (2010). piRNA-mediated silencing in Drosophila germlines. Semin. Cell Dev. Biol. *21*, 754–759.

Updike, D.L., Hachey, S.J., Kreher, J., and Strome, S. (2011). P granules extend the nuclear pore complex environment in the C. elegans germ line. J. Cell Biol. *192*, 939–948.

Zhao, R., Shen, J., Green, M.R., MacMorris, M., and Blumenthal, T. (2004). Crystal structure of UAP56, a DExD/H-box protein involved in pre-mRNA splicing and mRNA export. Structure *12*, 1373–1381.